Colloid and Polymer Science (2021) 299:999–1009
https://doi.org/10.1007/s00396-021-04823-8

ORIGINAL CONTRIBUTION

Stiffened and toughened polyacrylamide/polyanionic cellulose physical hydrogels mediated by ferric ions

Jianquan Wang[1] · Ying Ma[1] · Xiaofu Dai[1] · Baixue Gong[1] · Pan Chen[1] · Ziqiang Shao[1] · Xiaonan Huang[2]

Received: 28 August 2020 / Accepted: 25 January 2021 / Published online: 10 February 2021

Abstract

High-strength hydrogels have recently attracted many attentions owing to their potential applications in various fields. Yet, how to relive the contradiction between strength and ductility is still a challenge. In this work, a series of Fe(III)-crosslinked polyacrylamide/polyanionic cellulose composite physical hydrogels [PAM/PAC-Fe(III)] were firstly prepared via polymerizing acrylamide in PAC solution free of chemical crosslinkers, and followed by posttreatment in 0.1 M iron chloride solution. The obtained hydrogels were characterized by FTIR spectroscopy and scanning electron microscopy as well as tensile and compressive mechanics. Herein, the mechanics of PAM/PAC-Fe(III) hydrogels exhibits both stiffened and toughened properties, benefitting from the synergy between hydrogen bonding and Fe(III)-COO^- coordination interactions within the networks. Subsequently, their properties were compared with those of Zr(IV)- and cellulose nanofiber (CNF)-based analogues in our previous studies. Fe(III) species afford the hydrogels more flexibility than the Zr(IV) ones do due to the lower valency and weaker affinity of Fe(III) than those of Zr(IV); PAC-based systems demonstrate broader and/or higher mechanical reinforcement effects than CNF-based ones ascribing to higher carboxylate content and higher dosage of PAC than CNF. In brief, the present research provides an effective approach to fabricate simultaneously stiffened and toughened hydrogels and provides a guidance to rationally design metal-ion mediated PAM-based composite hydrogels.

Keywords Hydrogels · Polyacrylamide · Polyanionic cellulose · Ferric ions · Mechanical properties

Introduction

Hydrogels, a typical class of polymer networks containing a large amount of water, attracted much attention due to their potential applications as biomaterials including wound dressing, drug delivery, and bioscaffolds. However, these classes of materials had traditionally been regarded as weak and brittle materials originally. Recently, the exciting progress for strong hydrogels has gained via some novel strategies such as micro-/nano-composite [1–4], double networks [5], slide-ring crosslinks [6], homogeneous network [7], ionic bonding [8], hydrophobic association [9], and metal-ligand coordination [10, 11]. These strategies efficiently solve the fragile problems of hydrogels via dissipating energy and/or minimizing network defects, enabling their applications in extended fields such as load-bearing biomaterials [12], soft robotics [13], and wearable devices [14–16].

For enhancement of hydrogels, energy dissipation properties may be improved by reversible physical crosslinks. Cation-anion electrostatic attraction, a kind of common dynamic interaction, has been used to construct strong hydrogels. Two representative achievements are polyampholyte hydrogels and Ca^{2+}-crosslinked polyacrylamide/alginate hydrogels, in which both interactions of sulfonate-quaternary ammonium and Ca^{2+}-carboxylate groups contribute to extraordinary mechanical properties via energy dissipation mechanism, respectively [8, 17]. Further, Fe(III)-COO^- ion pair provides additional strong coordinate bonding power besides electrostatic attractions through the affinity between unfilled *d* orbitals of ferric ions and the lone electron pairs of carboxylates [18]. So this special couple has been broadly applied to the fabrication of high-performance hydrogels, achieving reinforced mechanics, rapid self-reversibility, and healing abilities [19–23].

✉ Jianquan Wang
jqwang@bit.edu.cn

[1] Beijing Engineering Research Center of Cellulose and Its Derivatives, School of Materials Science and Engineering, Beijing Institute of Technology, Beijing 100081, China

[2] Department of Chemistry, Capital Normal University, Beijing 100048, China

It is well known that cellulose is the most abundant and renewable nature materials on earth, and its traditional derivatives such as cellulose esters and ethers have been widely used in various fields of human daily life. In particular, nanocellulose products have recently gained many attentions due to their biodegradability, light weight, and high-strength natures. Generally, there are two types of carboxylated cellulose derivatives: carboxymethyl cellulose (CMC) and TEMPO-oxidized cellulose nanofibers (CNF), both of which can supply appreciable carboxylate groups to coordinate with multivalent cations. Their structural difference is as follows: CMC is in the form of single cellulose chains, whereas CNF is in the form of linear nanofibrils. Moreover, a type of advanced CMC product with more uniform substitution is usually called polyanionic cellulose (PAC). In our previous studies, we have used both CNF and PAC (carboxyl contents of 1.56 and 3.87 mmol/g, respectively) to fabricate composited polyacrylamide (PAM) hydrogels treated by Fe(III) and Zr(IV) species, respectively. For them, the synergy between hydrogen bonding and metal-ionic coordination interactions contributes to the enhancement of mechanics and other interesting properties [24, 25]. For example, the obtained PAM/CNF-Fe(III) hydrogels manifested improved ductility and stiffness as well as healing ability [24]; PAM/PAC-Zr(IV) hydrogels behaved high strength, favorable self-recovery, outstanding fatigue durability, and unexpected acid-resistance [25]. Still, PAM/CNF-Fe(III) hydrogels were restricted by the lower carboxylate content and limited dosage (only 2 wt% of AM maximum) of CNF, difficult to further reinforce; PAM/PAC-Zr(IV) ones achieved MPa-scale compressive strength but behaving only fourfold of elongation, too rigid to be fully extended. Hence, the contradiction between strength and ductility still needs to be relieved. In addition, carboxylated cellulose derivatives (CNF and PAC) and metal cations [Fe(III) and Zr(IV)] act as key elements of hydrogen bonding and metal coordination in PAM networks, and their structural effects on hydrogel properties also need analysis so as to guide the rational design of this species of metal mediated PAM-based composite hydrogels.

With the aim to simultaneously gain both stiffness and toughness for carboxylated cellulose-composited PAM hydrogels, we fabricated physical PAM/PAC composite hydrogels treated by ferric ions, PAM/PAC-Fe(III). Their mechanical properties were measured and then compared with the former hydrogel analogues [PAM/CNF-Fe(III) and PAM/PAC-Zr(IV)] previously reported by us. In our present and former studies, $FeCl_3$ and $ZrOCl_2$ aqueous solutions were used to treat the prepared primary hydrogels. There is a fact that both metal cations are not in the form of their respective free cations but hydrate clusters: $[Fe(H_2O)_6]^{3+}$, $[FeCl(H_2O)_5]^{2+}$ and $[FeCl_2(H_2O)_4]^{+}$ for ferric cations [26], and $[Zr_4(OH)_8(H_2O)_{16}]^{8+}$ for zirconic cations [27], we alternatively used Fe(III) and Zr(IV) instead of Fe^{3+} and Zr^{4+}, respectively.

Materials and methods

Materials

PAC with the degree of substitution (DS) of 0.91 (equal to 3.87 mmol/g) was synthesized through modified carboxymethylation of cellulose, as described in our previous paper [25]. Iron(III) chloride hexahydrate ($FeCl_3{\cdot}6H_2O$) was purchased from Tianjin Fuchen Chemical Factory, China. Acrylamide (AM, 98%) was supplied by Mitsui Chemicals, Japan. N, N, N′, N′-Tetramethylethylenediamine (TEMED) and ammonium persulfate (APS) were bought from Shanghai Richjoint Chemical Reagent Co. Ltd., China.

Fabrication of hydrogels

The same method as Zr(IV)-based hydrogel fabrication was performed in this research [25]. Briefly, PAM/PAC composite hydrogels were prepared as follows: 200 mg of AM was dissolved in the 780 μL of PAC aqueous solution, which was polymerized in different molds under the protection of N_2 atmosphere at 15 °C for 24 h. The system was initiated by 10 μL of 1.5 M TEMED and 10 μL of 0.15 M APS. In these systems, PAC contents were tuned from 0 to 6 wt% relative to AM amount according to different formulations. The obtained gel free of PAC was named PAM, and those containing PAC were nominated as PAC*x* (*x*=1.5, 3, 4.5, 6), where *x* represents the mass percentage of PAC to AM. Then Fe(III)-crosslinked hydrogels were produced via 12 h of immersion of as-prepared PAM/PAC gels in 0.1 M $FeCl_3$ aqueous solution and following equilibration in deionized water for 24 h at room temperature. Correspondingly, the resultant hydrogels were named as PAC*x*-Fe0.1 (*x*=1.5, 3, 4.5, 6), respectively.

For the prepared hydrogels, swelling ratio can be estimated using following equation.

$$\text{Swelling Ratio (g/g)} = W_e/W_0 \quad (1)$$

where W_0 is the wet weight of as-prepared gel after polymerization and W_e is the equilibrated weight of resultant Fe(III)-treated gel in deionized water for 24 h. For every recipe, at least 3 samples were measured and the average value was taken.

Measurements

Universal Testing Machine (Instron 5567-1 KN) was used to perform mechanical tests at room temperature. For compression tests, cylinder-shaped samples (h=13~18 mm, ϕ=13~16 mm) were compressed to the strain of 90 % with a rate of 2 mm/min; for tensile ones, tailored dumbbell-shaped specimens following Chinese Standards GB/T 528-2009 (shown in Fig. S1) were stretched to fracture using a rate of 40 mm/

min. For every sample, the values of stress and strain were calculated from the applied load divided by the original cross-sectional area of the sample and the clamp displacement divided by initial distance, respectively; modulus was taken from the slope of the stress-strain curve between a strain of 5 and 15%; and work of extension for tensile and toughness for compression were respectively recorded as the integral areas of the stress-strain curves. The dissipated energy was assessed in terms of the area between loading-unloading curves; accordingly, the energy dissipation ratio was calculated from the dissipated energy divided by the toughness of loading process. For accuracy, at least three valid data for each sample were provided, and the average values were taken.

The changes of hydrogen bonding involving amide groups were examined by Fourier Transform Infrared Spectrometry (FTIR, BRUKER TENSOR 27). The morphological observation was achieved by field-emission scanning electron microscope (SEM, Hitachi S-4800), for which the lyophilized gels were sputtered with gold before observation. The metal content of the gels was analyzed by inductively coupled plasma mass spectrometry (ICP-MS, iCAP Q, Thermo, Waltham), for which the lyophilized samples were used. Aqua regia was applied to digest the sample to get a solution with precise concentration, which was injected into the equipment for measurement; at least three samples for each formulation were analyzed, and the average values were adopted.

Results and discussion

Fabrication of composite hydrogels

As illustrated in Scheme 1, AM was polymerized through in situ radical polymerization in PAC aqueous solutions to get PAM/PAC composite gels; subsequently, the as-prepared gels were soaked in 0.1 M $FeCl_3$ aqueous solution for 12 h, followed by immersing in a large amount of deionized water for 24 h, achieving the equilibrium states of hydrogels. As for our previous PAM/PAC-Zr(IV) hydrogels, we found the PAC content exerted greater effect on hydrogel properties than metal concentrations, and 0.1 M of concentration is an appropriate value. Therefore, the influence of PAC dosage is studied in this work: a series of hydrogels with modulated PAC content, PAC*x*-Fe0.1(*x*=1.5, 3, 4.5, 6), were prepared. Meanwhile, pure PAM hydrogel was also produced as a control. The resultant PAC*x*-Fe0.1 hydrogels demonstrate different extents of swelling relative to the original as-prepared ones. As shown in Fig. 1a, swelling ratio, which was defined as the mass ratio of equilibrated hydrogel to as-prepared initial one, reveals obvious decrease with PAC dosage. Namely, swelling ratios reduce from 3.2 to 2.0 when PAC dosage rises from 1.5 to 6 wt% relative to AM amount; correspondingly, their water contents decrease from 94 to 89%, showing a relatively narrow range.

FTIR spectroscopy of representative samples such as PAM, PAC6 (PAM/PAC), and PAC6-Fe0.1 xerogels are shown in Fig. 1b. For PAM, the peaks at 3335, 3186 (N–H stretching vibration), 1649 (amide I), 1600 (amide II), and 1417 cm^{-1} (amide III) stand for characteristic absorptions of the -$CONH_2$ groups. Both peaks at 2935 and 1449 cm^{-1} correspond to -CH_2- stretching and bending vibrations, respectively [28–31]. After 6 wt% of PAC relative to AM was incorporated, the above five characteristic signals of −$CONH_2$ groups shift to 3326, 3181, 1646, 1608, and 1409 cm^{-1}, respectively, reflecting strong hydrogen bonding interaction between PAM and PAC chains ascribing to amide moieties on PAM and carboxyl/hydroxyls on PAC. For PAC6-Fe0.1, those five peaks related with −$CONH_2$ moieties further shift to 3331, 3189, 1648, 1603, and 1412 cm^{-1}, respectively, indicating some alternation of hydrogen bonding interactions inside gels after the treatment of $FeCl_3$ solutions.

Moreover, Fe contents in resultant xerogels were measured, and the corresponding carboxylate contents in gels were also estimated based on feeding amounts of AM and PAC, assuming complete conversion of AM in polymerization and negligible leakage in posttreatment. The respective contents of ferric ions, carboxylates, and their ratios are listed in Table 1. For the xerogels, Fe contents show a narrow range of 0.14–0.16 mmol/g, suggesting that $FeCl_3$ concentration of immersion solution is a decisive factor to Fe amounts entering into networks owing to the osmotic pressure difference between the gel interior and external environments. The molar ratios between ferric ions and carboxyls inside gels become less with the increasing PAC dosage, as revealed in Table 1. It has been reported that there exist three types of Fe(III)−COO^- coordinations such as mono-, bi-, and tridentates, among which the latter two can construct effective crosslinks and tridentate one is the most favorable to reinforce hydrogels [32]. Also for $FeCl_3$ aqueous solution, three types of hydrate clusters such as $[Fe(H_2O)_6]^{3+}$, $[FeCl(H_2O)_5]^{2+}$, and $[FeCl_2(H_2O)_4]^{+}$ were observed [26]. For effective crosslinks, the optimal ratio of ferric ions to carboxylates in networks should be one third. Actually, as shown in Table 1, the values are all well above one third, i.e., 2.5–7.5-folds of this optimum. The higher this ratio, the more mono-/bidentate styles of Fe(III). These incompletely crosslinked ferric ions must be accompanied with the fact that more water sorbed into networks in the last process for water equilibration. In this sense, the higher ratio of ferric ions to carboxylates will result in higher swelling ratio.

The hydrogen bonds between PAM and PAC chains inside networks are another notable factor, as demonstrated in FTIR (Fig. 1b). This interaction may be influenced by the acidity of interior environment and the low pH value of which induced the protonization transition from −COO^- to –COOH, in favor

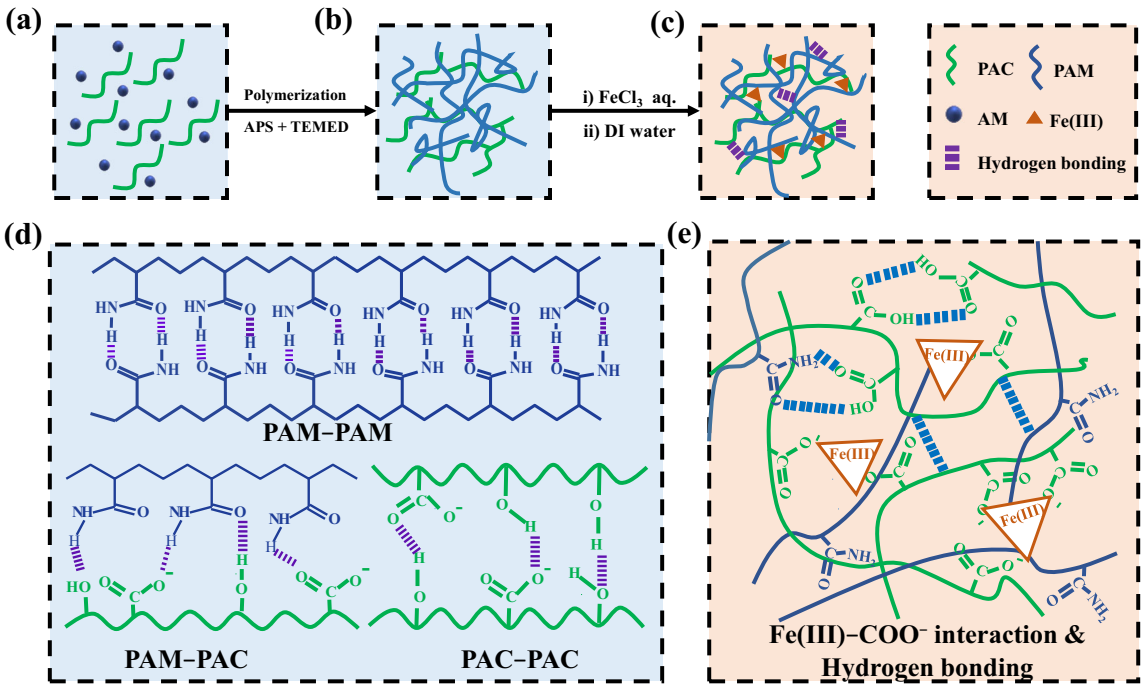

Scheme 1 Schematic illustration of PAM/PAC-Fe(III) hydrogels. (a)–(c) Preparation of the hydrogels, (d) Hydrogen bonding network involved in PAC and PAM polymer chains; (e) Coexistence of Fe(III)–COO^- coordination and hydrogen bonding

of the establishment of strong hydrogen bonding interactions. It has been reported that the pKa of CMC –COOHs varies from 4.8 to 5 [33], while pH value of $FeCl_3$ aqueous solution ranges from 2.5 to 1.0 with $FeCl_3$ concentration of 0.01 to 1 M [22]. Thus, so much lower pH value than pKa can protonize partial $-COO^-$ moieties, enhancing hydrogen bonding interaction involving −COOHs in the resultant gels. For PAC*x*-Fe0.1 systems treated with 0.1 M $FeCl_3$ solution, which have the same acidic environments as the gels, higher PAC dosage corresponds to relatively more carboxyl groups. This in turn increases the number of hydrogen bonds within the networks, in combination with lower ratio of ferric ions to carboxylates that means more tridentate Fe(III) coordination style as discussed above, so the resultant hydrogels with more PAC contents behave less swelling ratios.

In summary, both hydrogen-bonds and Fe(III)–COO^- coordinations constitute sole physical crosslinks in networks because no chemical cross-linkers were adopted in gel preparation and the degree of physical crosslink is positively related with the dosage of PAC. Moreover, the above results about swelling ratios, water contents of hydrogels, as well as metal contents in xerogels show the same trends with varied PAC dosage as those for PAM/PAC-Zr(IV) analogues in our former research [25]. For metal contents in xerogels, however,

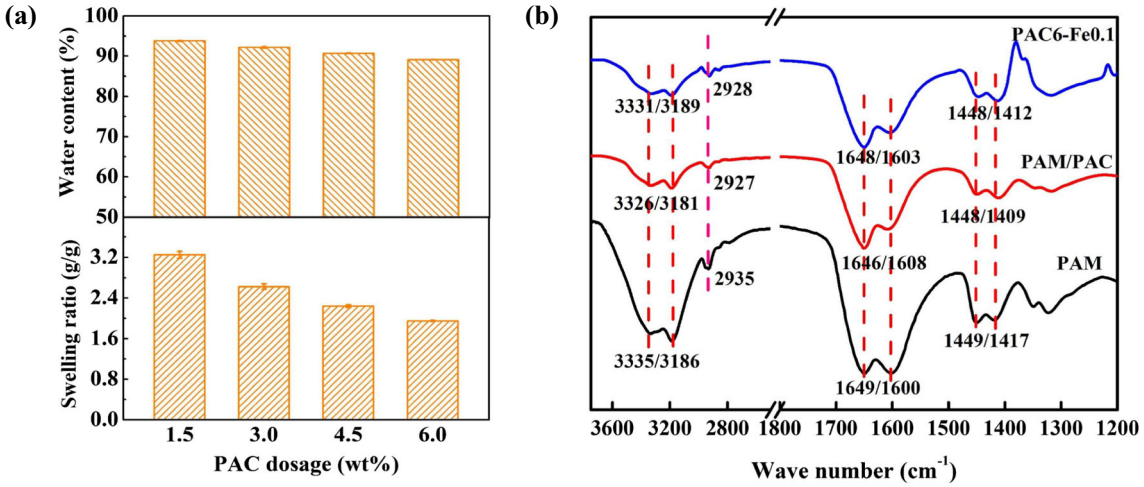

Fig. 1 **a** Swelling ratios of resultant PAC*x*-Fe0.1 gels relative to their corresponding as-prepared ones, and their water contents. **b** FTIR spectra of PAM, PAM/PAC, and PAC6-Fe0.1 xerogels

Table 1 Fe(III) and carboxylate contents in xerogels with different compositions

Samples	PAC1.5-Fe0.1	PAC3-Fe0.1	PAC4.5-Fe0.1	PAC6-Fe0.1
Fe(III) (mmol/g)	0.143 ± 0.001	0.144 ± 0.004	0.149 ± 0.002	0.163 ± 0.003
$-COO^-$ (mmol/g)	0.057	0.113	0.167	0.219
$n_{Fe(III)}/n_{COO^-}$ (mol/mol)	2.509	1.274	0.892	0.744

Zr(IV)-based ones are much higher than Fe(III)-ones: 0.45-0.52 mmol/g *vs* 0.14-0.16 mmol/g (around 3 times). This result may be associated with stronger binding affinity of Zr(IV) with PAC than Fe(III) clusters, which in turn leads to their difference in mechanical properties. This will be discussed in latter context.

Internal network structures

It has been known that both hydrogen bonding interaction and tridentate Fe(III)−COO^- coordinations can be enhanced by introducing more PAC into networks, consequently resulting in the slight reduction of water contents in gels. Thus the network structure inside gels may become relative denser with the augmentation of PAC dosage. SEM was used to characterize the internal network structures, as shown in Fig. 2. For the PAC1.5-Fe0.1 sample, the network is full of micrometer-scale large pores (Fig. 2a), whereas heterogeneous porous structure with coexistence of big and small pores emerges for the other hydrogels with PAC dosage of over 3 wt%. In PAC3-Fe0.1 gel, there appears a great number of nano-pores accompanied by some scattered μm-scale pores; simultaneously some interconnected and branched thin nanofibers can be detected as walls of some large pores (Fig. 2b). Then for PAC4.5- and PAC6-Fe0.1 gels, the nanofibers become thicker, as shown in Fig. 2c and d; meanwhile there appears the heterogeneous distribution of relative small pores inside the big ones surrounded by those thick nanofibers. Like the case of Zr(IV)-crosslinked PAM/PAC hydrogels, the interconnected and branched nanofibers distributed in networks probably suggest the formation of nanoscale assembly among polymer chains via the synergic effect between hydrogen bonding interaction and metal coordination. As a supplemental proof, Tyndall effect is observed for the transparent resultant PAC*x*-Fe0.1 gels, but not for their respective precursor PAC*x* (PAM/PAC) gels and 0.1 M $FeCl_3$ solution, as shown in Fig. 3. This phenomenon also provides a proof for the formation of nanoscale colloid assembles in networks after the incorporation of Fe(III), which may be achieved via the Fe(III)−COO^- coordination. Here, such an inference from SEM and Tyndall effect needs to be further verified using more convincing measurements such as cryo-transmission electron microscope, in situ atomic force microscope, small angle X-ray scattering, and small angle neutron scattering that will be carried out in future.

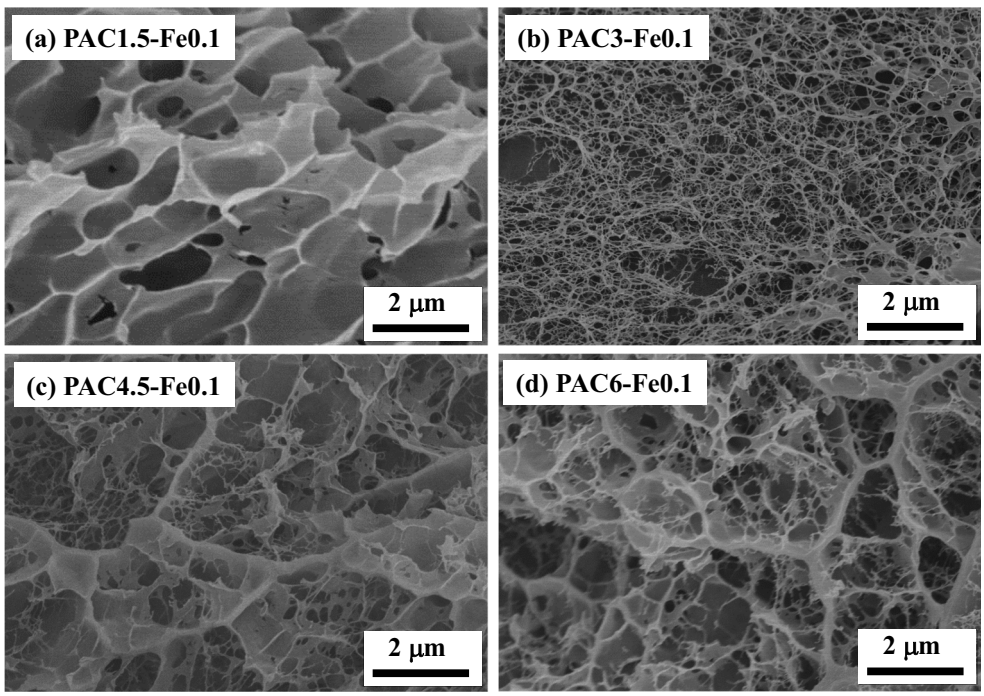

Fig. 2 SEM graphs of PAC*x*-Fe0.1 hydrogels

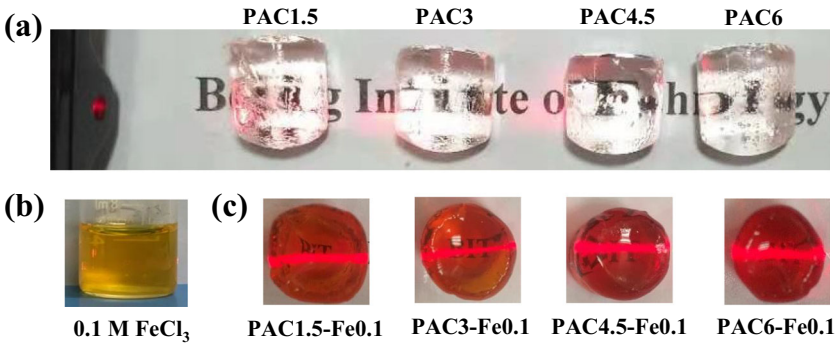

Fig. 3 Light beam passing experiment for (**a**) as-prepared PAC*x* hydrogels, (**b**) 0.1 M $FeCl_3$ solution, and (**c**) resultant PAC*x*-Fe0.1 hydrogels. No Tyndall effect was found for PAC*x* gels and $FeCl_3$ solution, while PAC*x*-Fe0.1 hydrogels demonstrate obvious Tyndall effect

Mechanical properties

Tensile and compressive mechanical properties were examined. Figure 4a, b, and c illustrate visual images of several representative hydrogels. The knotted PAC1.5-Fe0.1 sample with 5-mm thickness can be stretched to eightfold of its initial length. The gel PAC6-Fe0.1 can bear up to 1.5 kg of weight without breakage and can be compressed by 90% reversibly without any damage. The excellent mechanical performances are endowed by the synergy between hydrogen bonding and Fe(III) coordination inside gels. Figure 3d and e demonstrate typical tensile and compressive stress-strain curves of gels, respectively, from which one can find that the increase of PAC dosage favors the reinforcement of obtained hydrogels.

The tensile strength, Young's modulus, elongation at break, and work of extension as a function of PAC dosage are plotted in Fig. 5. Except the elongation at break, all other quantities reveal obvious increase along with the increase of PAC dosage. When PAC dosage rises from 1.5 to 6.0 wt%, tensile strength and Young's modulus achieve around 4- and 12-fold of increment, respectively, but elongation at break falls by 50%, subsequently leading to threefold of elevation for work of extension, i.e., 93 ± 12 kPa *vs* 410 ± 18 kPa, 35 ± 12 kPa *vs* 546 ± 34 kPa, 990 ± 60 *vs* 558 ± 20, and 532 ± 87 kJ·

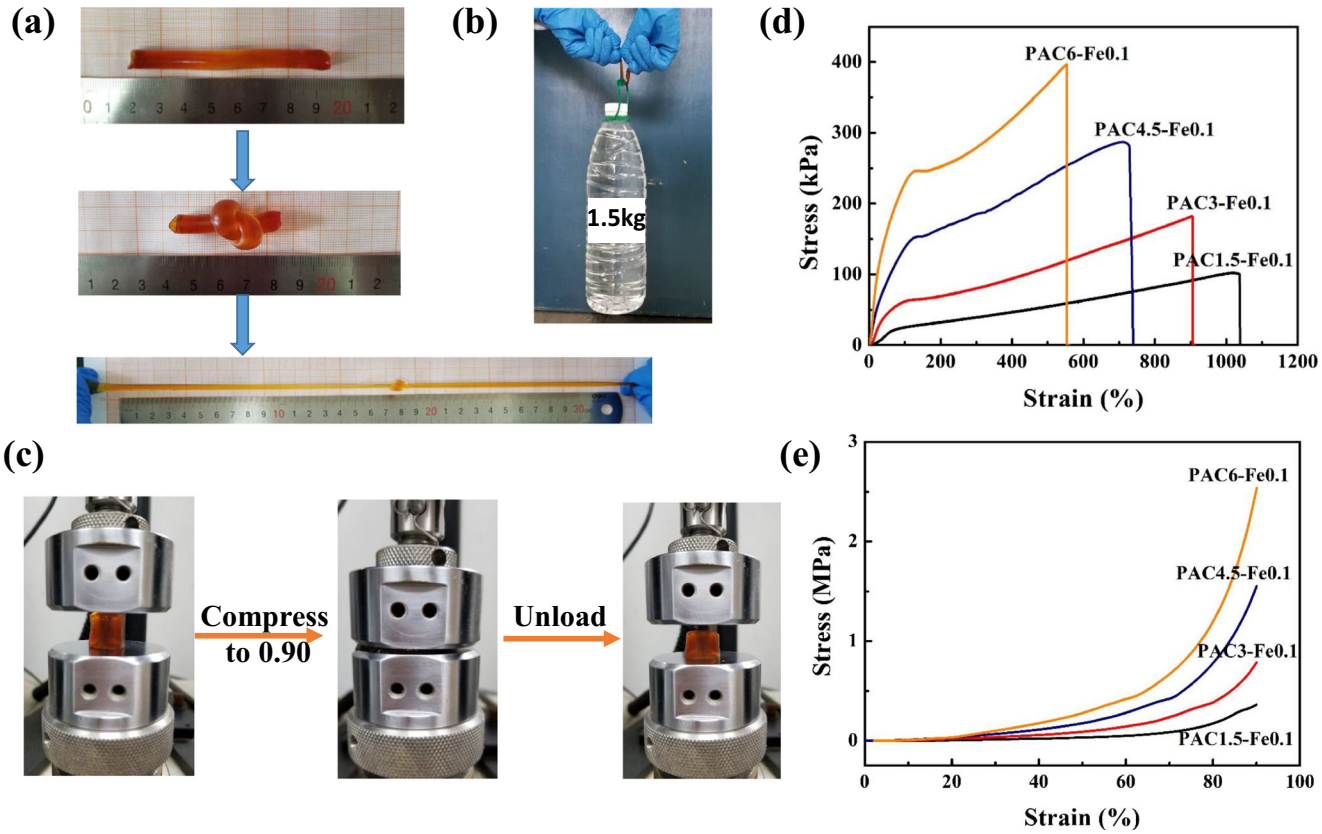

Fig. 4 Visual images of (**a**) knotted 5 mm-thick PAC1.5-Fe0.1 gel capable of being stretched to over 8 times of extension, (**b**) 5 mm-thick PAC6-Fe0.1 gel able to bear 1.5 kg of weight, (**c**) column PAC6-Fe0.1 gel before and after compression. Tensile (**d**) and compressive (**e**) stress-strain curves of PAC*x*-Fe0.1 gels

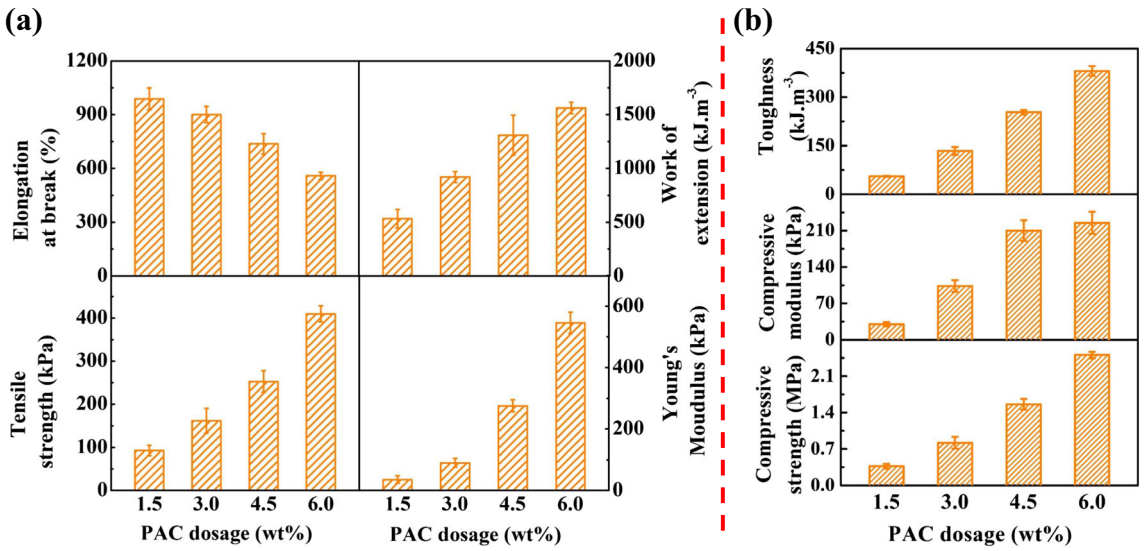

Fig. 5 Tensile (**a**) and compressive (**b**) data comparison for PAC*x*-Fe0.1 gels

m^{-3} *vs* 1562 ± 52 kJ·m^{-3}, respectively. Here, the elongations of Fe(III)-crosslinked PAM/PAC gels behave monotonous downward trend (10 to 5 times) with PAC dosage increasing and demonstrate higher ductility than Zr(IV)-based analogues in our previous research, where Zr(IV)-systems can be extended to only around 4 times independent of PAC dosage [25]. Thus, under the premise of the same PAC dosage, Fe(III)-based hydrogels in this study appear a bit higher tensile strength than Zr(IV)-based ones thanks to the improved elongation, as shown in Fig. S2. Higher ductility featured by Fe(III)-based gels than Zr(IV)-based ones may benefit from more flexible nature of Fe(III) than Zr(IV) clusters, which will be analyzed in latter context.

For compressive mechanics, as shown in Fig. 5b, compressive strength, modulus, and toughness are improved significantly by the increase of PAC dosage, similar to the case of tensile ones. For example, the values of compressive strength, modulus, and toughness at 90 % of deformation for PAC1.5-Fe0.1 are 0.36 ± 0.04 MPa, 30.0 ± 3.6 kPa, and 55.4 ± 1.7 kJ·m^{-3}, respectively; when PAC dosage rises to 6 wt% (PAC6-Fe0.1), the above three parameters reach 2.51 ± 0.17 MPa, 225 ± 21 kPa, and 381 ± 15 kJ·m^{-3}, respectively, attaining about sevenfold of increment for each parameter compared with those of PAC1.5-Fe0.1. Here, it is worth noting that PAC*x*-Fe0.1 hydrogels at PAC dosage of over 3 wt% have a compressive strength with a level of megapascal (0.8–2.5 MPa, Fig. 4b), even if 90 % of water is contained. In this sense, the hydrogels reported in this study still belong to the category of high-strength compression-resistant hydrogels. After all, only few literatures have published megapascal grade compression-resistant hydrogels hitherto [34–39]. In comparison with those of Zr(IV)-based analogues, these compression mechanical values are lower at the same of PAC dosage, as shown in Fig. S3, which is contrary to that of tensile properties.

Further, single cyclic compressive mechanics were performed to explore energy dissipation mechanism of obtained hydrogels. The initial loading-unloading curves are shown in Fig. 6a. One can find pronounced hysteresis phenomenon that reflects energy dissipation mechanism. For the tough hydrogels, the area of hysteresis loop is defined as dissipated energy. Correspondingly, its ratio to the total energy of loading process is considered to be energy dissipation ratio [40]. Figure 6b reveals energy dissipation of hydrogels with different recipes. The dissipated energy increases obviously with PAC dosage. Here, PAC plays an important role in energy dissipation capacity due to the contribution from hydrogen bonds and metal coordination, both of which act as reversible crosslinks within networks. Thus the augmentation of PAC dosage from 1.5 to 6.0 wt% led to the jump of dissipated energy from 22.6 ± 2.2 to 191.5 ± 22.8 kJ·m^{-3}, achieving around as high as ninefold of increment, as shown in Fig. 6b. In comparison with Zr(IV)-based analogues, whose dissipated energy values ranged from 28.6 ± 5.0 to 260.5 ± 37.4 kJ·m^{-3}, Fe(III)-based hydrogels appeared lower values at the same PAC dosage [25]. In addition, the obtained hydrogels in this research demonstrate energy dissipation ratios with a narrow scope of 70–80 %, indicating their high dissipation efficiencies.

The mechanical properties of PAM/PAC-Fe(III) hydrogels in this study were compared with PAM/CNF-Fe(III) gels in our previous research, as shown in Fig. S4 and S5. Here the data ranges of enhanced hydrogels are compared because of the inconformity of their dosages. It can be seen that, for tensile and compressive tests, PAC-based hydrogels generally display broader scopes and/or higher values than CNF-based ones for the values of strength, modulus, and work of extension or toughness, except for that the former systems show narrow range for elongation at breaks.

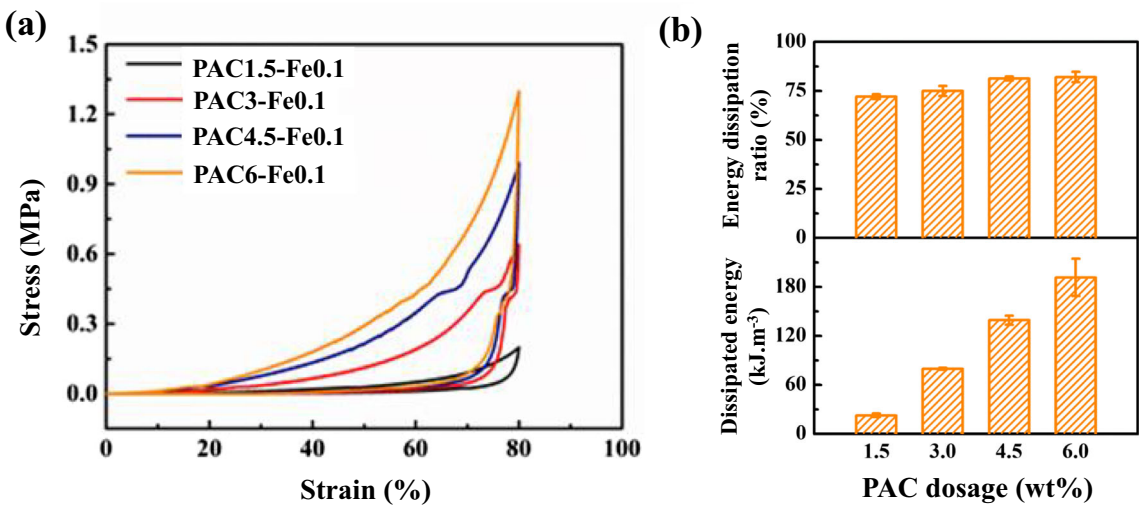

Fig. 6 Single loading-unloading cyclic compression curves for PAC*x*-Fe0.1 gels (**a**) and their energy dissipation comparison (**b**)

Analysis of differences between PAM/PAC-Fe(III) and Zr(IV)-/CNF-based analogues

As discussed above, reversible dynamic crosslinks such as hydrogen bonding and Fe(III)-COO^- interactions inside PAM/PAC-Fe(III) hydrogels take responsible for their energy dissipation. When subjected to external forces, the scission of reversible physical interactions absorbs mechanical energies, endowing the hydrogels with both enhanced stiffness and toughness. Here the property differences between PAM/PAC-Fe(III) and Zr(IV)-/CNF-based analogues are analyzed, in order to better understand the structural effects from ferric and zirconic ions as well as that from PAC and CNF.

In the above section, some differences between Fe(III)- and Zr(IV)-crosslinked PAM/PAC hydrogels have been mentioned, i.e., Fe(III)-based ones behave higher ductility and tensile strength but lower compressive strength and dissipated energy than Zr(IV)-based analogues at the same PAC dosage. This result must be associated with the structural natures of both cations as well as their interactions with $–COO^-$ groups in networks. It has been known that hydrate clusters are the main forms of Fe(III) and Zr(IV) cations in their respective $FeCl_3$ and $ZrOCl_2$ aqueous solutions. There exist three types of clusters such as $[Fe(H_2O)_6]^{3+}$, $[FeCl(H_2O)_5]^{2+}$ and $[FeCl_2(H_2O)_4]^+$ for ferric cations [26] and one major type of $[Zr_4(OH)_8(H_2O)_{16}]^{8+}$ clusters for zirconic cations [27]. When these clusters penetrated into PAM/PAC networks during posttreatment in salt solutions, they would interact with $–COO^-$ groups through ionic coordination, and some clusters might be destroyed due to the competition from $–COO^-$ moieties on PAC chains. Comparing Fe(III) and Zr(IV) ions/clusters, the former ones have lower valencies and smaller sizes than the latter. The highest valency of Fe(III) clusters is +3, meaning that one ion/cluster can bond three carboxylates at most, while one Zr(IV) cluster with +8 valency can supply eight bonding sites to interact with carboxylates. In this sense, Fe(III) clusters may behave more flexible nature in networks ascribing to weaker binding force and smaller sizes than Zr(IV) ones. Actually the strong binding affinity of Zr(IV) ions/clusters to PAC chains and consequent inactivity in networks have been proved by ethylene diamine tetraacetic acid disodium salt (EDTA·2Na) chelation experiment in our previous research, which demonstrated that Fe(III)-based hydrogels had been dissolved, while Zr(IV)-based ones still kept their integrity and remained about 1/3 of Zr(IV) amount after treated by saturated EDTA·2Na solution [25]. In addition, higher metal contents and acid-resistance featured for Zr(IV)-based gels than Fe(III)-based gels also support the above opinion. The difference in valencies and structures of Fe(III) and Zr(IV) ion/clusters affects the macroscopic mechanical properties of hydrogels. Namely, Fe(III)-crosslinked hydrogels obviously reveal more ductile property than Zr(IV) ones, while the latter display stronger stress tolerance than the former, as shown by tensile and compressive experiments (Figs. S2 & S3), respectively.

For Fe(III)-crosslinked PAM/PAC and PAM/CNF hydrogels, the former systems show broader and/or higher mechanical strength and modulus than the latter. Such a result should stem from the low carboxylate content of CNF and its low dosage in recipes that limitedly supplied the numbers of hydrogen bonds and ionic coordination, leading to the reinforcement of composited PAM hydrogels to a limited extent, whereas, in comparison with molecular PAC, nanostructured CNF contribute to better ductility and unique CNF dispersion-assisted healing ability [24]. In fact, the prepared PAM/PAC-Fe(III) hydrogels were also tried to heal through several methods such as direct contact, gluing with water, PAC solution and even CNF dispersion, but none of them succeeded. The non-healing behavior may be associated with the rigid backbone of PAC and insufficient free ferric ions in the

obtained hydrogels which have been subjected to extracting in the last step for water equilibration. It was reported that self-healing ability of PAM composite hydrogels based on metal-ion mediation and hydrophobic association is affected by two aspects: free ferric ions could promote the healing of hydrogels, while carboxylate-containing rigid polysaccharide chains such as alginate and xanthan gum play negative roles in healing properties [41, 42]. On the contrary, Fe(III)-mediated poly(acrylic acid) (PAA)-based hydrogels demonstrate excellent healable properties due to the flexible nature of PAA backbone [22, 23, 43]. For PAM/CNF-Fe(III) hydrogels in our previous study, there should exist a great deal of free ferric ions in hydrogel networks because Fe(III) concentrations for posttreatment ranged from 0.5 to 2.0 M that were much higher than that used in this research (0.1 M), and also they had not undergone the further posttreatment in deionized water to remove free components; therefore the CNF-based hydrogels demonstrate healing behavior in spite of having more rigid and thicker chains than PAC. According to the above analysis, it can be inferred that non-healing PAM/PAC-Fe(III) systems may become healable if introducing some AA to participate in polymerization or greatly increasing the concentration of $FeCl_3$ solution for posttreatment and omitting the last step for water equilibration.

Conclusions

In consideration of some drawbacks of PAM/CNF-Fe(III) and PAM/PAC-Zr(IV) hydrogels, this work was performed with the purpose of relieving the contradiction between strength and ductility of them. Herein, benefitting from the synergic action of hydrogen bonding and Fe(III)-COO^- coordination, the tensile and compressive mechanics of PAM/PAC-Fe(III) physical hydrogels exhibit stiffened and toughened performances as well as facile adjustability. In addition, the internal network structures of gels are also dependent on PAC dosages, and higher PAC content favors the formation of heterogeneous porous structure and nanofibers. In the further comparison study with Zr- and CNF-based analogues, we find that Fe(III) species manifest more flexible nature than Zr(IV) ones and PAC-based systems demonstrate broader and/or higher mechanical reinforcement effects than CNF-based ones due to the higher carboxylate content on PAC and its higher dosage. In addition, the lack of healing ability of PAC-based hydrogels is analyzed, and some prediction is given. In summary, the present research provides a valid strategy to fabricate simultaneously stiffened and toughened hydrogels with broader mechanics ranges, and offers a guidance to rationally design metal-ion mediated PAM-based composite hydrogels.

Supplementary Information The online version contains supplementary material available at https://doi.org/10.1007/s00396-021-04823-8.

Funding This study was financially supported by National Natural Science Foundation of China (21004005), Beijing Municipal Natural Science Foundation (2204096), and Beijing Institute of Technology Research Fund Program for young scholars as well as the BIT-Belarus joint grants (BITBLR2020001).

Declarations

Conflict of interest The authors declare that they have no conflict of interest.

References

1. Huang T, Xu H, Jiao K, Zhu L, Brown HR, Wang H (2007) A novel hydrogel with high mechanical strength: a macromolecular microsphere composite hydrogel. Adv Mater 19:1622–1626. https://doi.org/10.1002/adma.200602533
2. Thoniyot P, Tan MJ, Karim AA, Young DJ, Loh XJ (2015) Nanoparticle-hydrogel composites: concept, design, and applications of these promising, multi-functional materials. Adv Sci 2: 1400010. https://doi.org/10.1002/advs.201400010
3. Volkan C, Zdravko K, Valentin R, Nikolai S, Miriam S, Ben K, Justus J, Jürgen PR, Matthias B (2016) Nanostructural evolution and self-healing mechanism of micellar hydrogels. Macromolecules 49(6):2281–2287. https://doi.org/10.1021/acs.macromol.6b00156
4. Haraguchi K (2007) Nanocomposite hydrogels. Curr Opin Solid State Mater Sci 11:47–54. https://doi.org/10.1016/j.cossms.2008.05.001
5. Gong JP, Katsuyama Y, Kurokawa T, Osada Y (2003) Double-network hydrogels with extremely high mechanical strength. Adv Mater 15:1155–1158. https://doi.org/10.1002/adma.200304907
6. Okumura Y, Ito K (2001) The polyrotaxane gel: a topological gel by figure-of-eight cross-links. Adv Mater 13:485–487.10.1002/1521-4095(200104)13:7<485::AID-ADMA485>3.0.CO;2-T
7. Sakai T, Matsunaga T, Yamamoto Y, Ito C, Yoshida R, Suzuki S, Sasaki N, Shibayama M, Chung UI (2008) Design and fabrication of a high-strength hydrogel with ideally homogeneous network structure from tetrahedron-like macromonomers. Macromolecules 41:5379–5384. https://doi.org/10.1021/ma800476x
8. Sun TL, Kurokawa T, Kuroda S, Ihsan AB, Akasaki T, Sato K, Haque MA, Nakajima T, Gong JP (2013) Physical hydrogels composed of polyampholytes demonstrate high toughness and viscoelasticity. Nat Mater 12:932–937. https://doi.org/10.1038/nmat3713
9. Oliveira NM, Zhang YS, Ju J, Chen AZ, Chen Y, Sonkusale SR, Dokmeci MR, Reis RL, Mano JF, Khademhosseini A (2016) Hydrophobic hydrogels: towards construction of floating (bio)microdevices. Chem Mater 28:3641–3648. https://doi.org/10.1021/acs.chemmater.5b04445
10. Zhong M, Liu YT, Liu XY, Shi FK, Xie XM (2016) Dually cross-linked single network poly(acrylic acid) hydrogels with superior mechanical properties and water absorbency. Soft Matter 12: 5420–5428. https://doi.org/10.1039/c6sm00242k
11. Hou S, Ma PX (2015) Stimuli-responsive supramolecular hydrogels with high extensibility and fast self-healing via precoordinated mussel-inspired chemistry. Chem Mater 27:7627–7635. https://doi.org/10.1021/acs.chemmater.5b02839
12. Bodugoz-Senturk H, Macias CE, Kung JH, Muratoglu OK (2009) Poly(vinyl alcohol)-acrylamide hydrogels as load-bearing cartilage substitute. Biomaterials 30:589–596. https://doi.org/10.1016/j.biomaterials.2008.10.010

13. Rao P, Sun TL, Chen L, Takahashi R, Shinohara G, Guo H, King DR, Kurokawa T, Gong JP (2018) Tough hydrogels with fast, strong, and reversible underwater adhesion based on a multiscale design. Adv Mater 30:e1801884. https://doi.org/10.1002/adma.201801884
14. Huang Y, Zhong M, Huang Y, Zhu M, Pei Z, Wang Z, Wang Z, Xue Q, Xie X, Zhi C (2015) A self-healable and highly stretchable supercapacitor based on a dual crosslinked polyelectrolyte. Nat. Commun. 6:10310. https://doi.org/10.1038/ncomms10310
15. Billiet T, Vandenhaute M, Schelfhout J, Vlierberghe SV, Dubruel P (2012) A review of trends and limitations in hydrogel-rapid prototyping for tissue engineering. Biomaterials. 33:6020–6041. https://doi.org/10.1016/j.biomaterials.2012.04.050
16. Huang Y, Zhong M, Shi F, Liu X, Tang Z, Wang Y, Huang Y, Hou H, Xie X, Zhi C (2017) An intrinsically stretchable and compressible supercapacitor containing a polyacrylamide hydrogel electrolyte. Angew Chem Int Ed 56:9141–9145. https://doi.org/10.1002/ange.201705212
17. Sun JY, Zhao X, Illeperuma WRK, Chaudhuri O, Oh KH, Mooney DJ, Vlassak JJ, Suo Z (2012) Highly stretchable and tough hydrogels. Nature 489:133–136. https://doi.org/10.1038/nature11409
18. Williams KS, Andzelm JW, Dong H, Snyder JF (2014) DFT study of metal cation-induced hydrogelation of cellulose nanofibrils. Cellulose 21:1091–1101. https://doi.org/10.1007/s10570-014-0254-y
19. Wang XH, Song F, Qian D, He YD, Nie WC, Wang XL, Wang YZ (2018) Strong and tough fully physically crosslinked double network hydrogels with tunable mechanics and high self-healing performance. Chem Eng J 349:588–594. https://doi.org/10.1016/j.cej.2018.05.081
20. Chen Q, Yan X, Zhu L, Chen H, Jiang B, Wei D, Huang L, Yang J, Liu B, Zheng J (2016) Improvement of mechanical strength and fatigue resistance of double network hydrogels by ionic coordination interactions. Chem Mater 28:5710–5720. https://doi.org/10.1021/acs.chemmater.6b01920
21. Liang Y, Xue J, Du B, Nie J (2019) Ultrastiff, tough, and healable ionic–hydrogen bond cross-linked hydrogels and their uses as building blocks to construct complex hydrogel structures. ACS Appl Mater Interfaces 11:5441–5454. https://doi.org/10.1021/acsami.8b20520
22. Zheng SY, Ding H, Qian J, Yin J, Wu ZL, Song Y, Zheng Q (2016) Metal-coordination complexes mediated physical hydrogels with high toughness, stick-slip tearing behavior, and good processability. Macromolecules 49:9637–9646. https://doi.org/10.1021/acs.macromol.6b02150
23. Chen W, Bu Y, Li D, Liu Y, Chen G, Wan X, Li N (2020) Development of high-strength, tough, and self-healing carboxymethyl guar gum-based hydrogels for human motion detection. Journal of Materials Chemistry C 8(3):900–908. https://doi.org/10.1039/C9TC05797H
24. Niu J, Wang J, Dai X, Shao Z, Huang X (2018) Dual physically crosslinked healable polyacrylamide/cellulose nanofibers nanocomposite hydrogels with excellent mechanical properties. Carbohydr Polym 193:73–81. https://doi.org/10.1016/j.carbpol.2018.03.086
25. Dai X, Wang J, Teng F, Shao Z, Huang X (2019) Zr(IV)-crosslinked polyacrylamide/polyanionic cellulose composite hydrogels with high strength and unique acid resistance. J Polym Sci B Polym Phys 57:981–991. https://doi.org/10.1002/polb.24853
26. Persson I (2018) Ferric chloride complexes in aqueous solution: an EXAFS study. J Solution Chem 47:797–805. https://doi.org/10.1007/s10953-018-0756-6
27. Nikoofar K, Khademi Z (2016) A review on green lewis acids: zirconium(IV) oxydichloride octahydrate ($ZrOCl_2{\cdot}8H_2O$) and zirconium(IV) tetrachloride ($ZrCl_4$) in organic chemistry. Res Chem Intermed 42:3929–3977. https://doi.org/10.1007/s11164-015-2260-6
28. Liu Y, Lee BP (2016) Recovery property of double-network hydrogel containing a mussel-inspired adhesive moiety and nano-silicate. J Mater Chem B 4:6534–6540. https://doi.org/10.1039/c6tb01828a
29. Sen G, Mishra S, Jha U, Pal S (2010) Microwave initiated synthesis of polyacrylamide grafted guar gum (GG-g-PAM)-characterizations and application as matrix for controlled release of 5-amino salicylic acid. Int J Biol Macromol 47:164–170. https://doi.org/10.1016/j.ijbiomac.2010.05.004
30. Zhou C, Wu Q, Yue Y, Zhang Q (2011) Application of rod-shaped cellulose nanocrystals in polyacrylamide hydrogels. J Colloid Interface Sci 353:116–123. https://doi.org/10.1016/j.jcis.2010.09.035
31. Sivanantham M, Kesavamoorthy R, Sairam TN, Sabharwal KN, Raj B (2008) Stimulus response and molecular structural modification of polyacrylamide gel in nitric acid: a study by Raman, FTIR, and photoluminescence techniques. J Polym Sci B Polym Phys 46:710–720. https://doi.org/10.1002/polb.21402
32. Hu Y, Du Z, Deng X, Wang T, Yang Z, Zhou W, Wang C (2016) Dual physically cross-linked hydrogels with high stretchability, toughness, and good self-recoverability. Macromolecules 49:5660–5668. https://doi.org/10.1021/acs.macromol.6b00584
33. Trivedi HC, Patel CK, Patel RD (1981) Studies on carboxymethylated cellulose: potentiometric titrations, 1. Macromol Chem Phys 182:3561–3567. https://doi.org/10.1002/macp.1981.021821218
34. Harrass K, Krüger R, Möller M, Albrecht K, Groll J (2013) Mechanically strong hydrogels with reversible behaviour under cyclic compression with mpa loading. Soft Matter 9:2869–2877. https://doi.org/10.1039/c2sm27603h
35. Nakayama A, Kakugo A, Gong JP, Osada Y, Takai M, Erata T, Kawano S (2004) High mechanical strength double-network hydrogel with bacterial cellulose. Adv Funct Mater 14:1124–1128. https://doi.org/10.1002/adfm.200305197
36. Qin X, Zhao F, Liu Y, Wang H, Feng S (2009) High mechanical strength hydrogels preparation using hydrophilic reactive microgels as crosslinking agents. Colloid Polym Sci 287:621–625. https://doi.org/10.1007/s00396-009-2018-z
37. Deng Y, Hussain I, Kang M, Li K, Yao F, Liu S (2018) Self-recoverable and mechanical-reinforced hydrogel based on hydrophobic interaction with self-healable and conductive properties. Chem Eng J 353:900–910. https://doi.org/10.1016/j.cej.2018.07.187
38. Li X, Qin H, Zhang X, Guo Z (2019) Triple-network hydrogels with high strength, low friction and self-healing by chemical-physical crosslinking. J Colloid Interface Sci 556:549–556. https://doi.org/10.1016/j.jcis.2019.08.100
39. Hua D, Gao S, Zhang M, Ma W, Huang C (2020) A novel xanthan gum-based conductive hydrogel with excellent mechanical, biocompatible, and self-healing performances. Carbohydrate Polymers 247:116743. https://doi.org/10.1016/j.carbpol.2020.116743
40. Shao C, Chang H, Wang M, Xu F, Yang J (2017) High-strength, tough, and self-healing nanocomposite physical hydrogels based on the synergistic effects of dynamic hydrogen bond and dual coordination bonds. ACS Appl Mater Interfaces 9:28305–28318. https://doi.org/10.1021/acsami.7b09614
41. Yuan N, Xu L, Wang H, Fu Y, Zhang Z, Liu L, Wang C, Zhao J, Rong J (2016) Dual physically cross-linked double network hydrogels with high mechanical strength, fatigue resistance, notch-insensitivity, and self-healing properties. ACS Appl Mater Interfaces 8(49):34034–34044. https://doi.org/10.1021/acsami.6b12243
42. Zheng Q, Zhao L, Wang J, Wang S, Liu Y, Liu X (2020) High-strength and high-toughness sodium alginate/polyacrylamide

double physically crosslinked network hydrogel with superior self-healing and self-recovery properties prepared by a one-pot method. Colloid Surfaces A 589:124402. https://doi.org/10.1016/j.colsurfa.2019.124402

43. Wei Z, He J, Liang T, Oh H, Athas J, Tong Z, Wang C, Nie Z (2013) Autonomous self-healing of poly (acrylic acid) hydrogels induced by the migration of ferric ions. Polym Chem 4(17):4601–4605. https://doi.org/10.1039/C3PY00692A